A New Boundary Integral Approach to the Determination of the Resonant Modes of Arbitrarily Shaped Cavities

Paolo Arcioni, *Member, IEEE*, Marco Bressan, *Member, IEEE*, and Luca Perregrini

***Abstract*—We present an efficient algorithm to determine the resonant frequencies and the normalized modal fields of arbitrarily shaped cavity resonators filled with a lossless, isotropic, and homogeneous medium. The algorithm is based on the boundary integral method (BIM). The unknown current flowing on the cavity wall is considered inside a spherical resonator, rather than in free-space, as it is usual in the standard BIM. The electric field is expressed using the Green's function of the spherical resonator, approximated by a real rational function of the frequency. Consequently, the discretized problem can be cast into the form of a real matrix linear eigenvalue problem, whose eigenvalues and eigenvectors yield the resonant frequencies and the associated modal currents. Since the algorithm does not require any frequency-by-frequency recalculation of the system matrices, computing time is much shorter than in the standard BIM, especially when many resonances must be found.**

I. Introduction

COMPUTER codes for the electromagnetic analysis of arbitrarily shaped cavities are very important for many applications, in particular for the design of interaction structures for particle accelerators. The design of accelerating cavities results in complicated shapes, that are obtained carrying on repeated analyses to optimize a number of parameters, such as Q-factors, beam coupling impedances, higher-order-mode spectrum, and so on. The interest in the calculation of many normalized modes derives also from the important role they play in the eigenvector expansion of the electromagnetic field in a closed region. Some recent algorithms for the wide-band analysis of waveguide junctions [1], [2] and for the characterization of special accelerating structures [3] are based on these expansions; their practical use requires the efficient and reliable calculation of a number of modes in fairly short times.

Available codes (see, for instance [4]–[7]) are usually based on the finite element or the finite difference method. Since these methods follow from the discretization of the field equations in differential form, they require a 3-D mesh and, consequently, a large memory allocation and a long computing time. When the medium inside the cavity is homogeneous, the number of the unknowns reduces dramatically using the boundary integral method (BIM), that requires a surface mesh.

Manuscript received June 29, 1994; revised April 24, 1995. This work was supported in part by INFN and the Italian National Research Council (CNR) Contract 92.02857.CT07.

The authors are with the Department of Electronics of the University of Pavia, I-27100 Pavia, Italy.

IEEE Log Number 9412687.

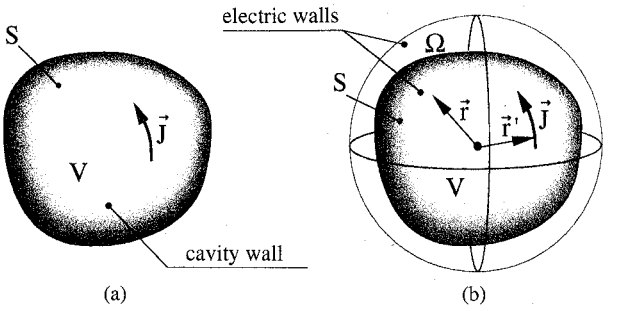

Fig. 1. The geometry of the problem. (a) A resonant cavity; (b) the same cavity embedded inside an external resonator.

The BIM is based on the solution of the homogeneous integral equation obtained by enforcing the electric-wall condition on the electric (or magnetic) field produced by the unknown wall-current $\vec{J}$ at an unknown frequency ω [Fig. 1(a)]. The method of moments (MoM) is used to transform the integral equation into a matrix eigenvalue problem, whose eigenvalues ω_r and eigensolutions $\vec{J}_r$ represent the resonant frequencies and the modal currents.

Usually, the unknown current is supposed to radiate in free-space, so that the kernel of the integral equation is the free-space Green's function, that is a transcendental complex function of the frequency. For this reason the standard BIM results in the solution of a nonlinear eigenvalue problem, which requires the search of the zeros of the determinant of a frequency-dependent complex matrix [8]. Thus, each resonance must be found through an iterative procedure based on the repeated evaluation of the MoM matrix and of its determinant at closely spaced frequencies in order to find the zeros. Unfortunately, no automatic procedure exists for the zero location and some *a priori* guess is unavoidable [9]. When many resonances must be found, not only may this lead to overlong computing times, but also some zeros (and consequently some modes) are possibly missed, especially in case of degenerate or nearly-degenerate modes. Furthermore, when normalized fields are needed, it is necessary to find the field generated by each $\vec{J}_r$ at a very large number of points to evaluate numerically the volume integral involved in the normalization of the modes. All these drawbacks may overwhelm the intrinsic advantages of using the BIM.

To overcome these shortcomings we follow a somewhat different formulation. We consider the unknown current $\vec{J}$ acting, rather than in free-space, inside a spherical volume

including the cavity and bounded by an electric wall [see Fig. 1(b)]. This is possible because, when ω corresponds to one of the resonant frequencies and $\vec{J}$ corresponds to the relative modal current, the field outside V is zero and therefore it does not matter what boundary condition we impose on the exterior field. Though "exotic" at first glance, this approach is convenient for two reasons. The most evident one is that the Green's function of the spherical resonator is real, thus leading to real MoM matrices. The second reason—actually the most important, though less apparent—derives from the fact that the Green's function of the spherical resonator can be approximated very well by a rational function of the frequency [10], a feature that permits us to find the eigensolutions by solving a linear matrix eigenvalue problem. Therefore, after a *single* evaluation of the MoM matrices, the resonant frequencies and the modal currents for all the modes of interest are found using well established and reliable procedures, that do not require any *a priori* guess of the resonant frequencies. Last but not least, the mode normalization is a trivial task, since it is possible to express the volume integrals of the modal fields as simple quadratic forms involving the eigenvectors and the MoM matrices. The efficiency of this approach has been already demonstrated in [11], where the same philosophy was followed for finding resonant frequencies of 2-D resonators.

Some preliminary results were presented in two recent symposium contributions [12], [13], where the method was only briefly outlined: the present paper is devoted to the comprehensive description of the algorithm (Section II) and of its implementation in a computer code (Section III). Some numerical results are reported in Section IV.

II. The Mathematical Formulation

A. Representation of the Field

Let V be the volume of the cavity, filled by a medium characterized by real, constant ϵ and μ [Fig. 1(a)]. Let us consider a spherical volume Ω bounded by an electric wall, including V and containing the same medium [Fig. 1(b)]. The field generated in Ω by the current sheet $\vec{J}$, defined over the cavity wall S, can be represented as follows [10]:

$$\vec{E} = -\nabla\Phi - j\omega\vec{A} \;\; ; \quad \vec{H} = \frac{\nabla \times \vec{A}}{\mu} \tag{1}$$

$$\Phi(\vec{r}) = \frac{1}{\epsilon}\int_S g(\vec{r},\vec{r}\,')\sigma(\vec{r})\,dS' \tag{2}$$

$$\vec{A}(\vec{r}) = \mu\int_S \overleftrightarrow{G}(\vec{r},\vec{r}\,')\cdot\vec{J}(\vec{r}\,')\,dS' + \mu k^2\sum_m \frac{\vec{e}_m(\vec{r})}{\kappa_m^2(\kappa_m^2-k^2)}\int_S \vec{e}_m(\vec{r}\,')\cdot\vec{J}(\vec{r}\,')\,dS' \tag{3}$$

where

- Φ and $\vec{A}$ are the scalar and vector potentials in the Coulomb gauge;
- $k = \omega\sqrt{\epsilon\mu}$ is the wavenumber;
- $\vec{r}$ and $\vec{r}\,'$ ($\vec{r}\,' \in S$) are the position vectors of the observation and source points, respectively;
- σ is the surface charge density (related to $\vec{J}$ by the continuity equation);
- g and $\overleftrightarrow{G}$ are the Green's functions for the quasi-static scalar and vector potential in the spherical cavity;
- κ_m is the resonant wavenumber of the mth mode of the spherical resonator and $\vec{e}_m$ is the corresponding electric field vector, normalized according to $\int_\Omega \vec{e}_m\cdot\vec{e}_m\,dV = 1$.

Functions $g, \overleftrightarrow{G}$, and $\vec{e}_m$ are real and k-independent; the expressions of $\vec{e}_m$ are found in many textbooks (e.g., [14, pp. 306–307]); the expressions of g and $\overleftrightarrow{G}$ are known in closed form and they are reported in the Appendix, Section A, in a form slightly different from that found in [10], best suited for numerical evaluation. Since the quasi-static dyadic $\overleftrightarrow{G}$ has the same singularity as the Green's function for vector potential [15], the quasi-static term in (3) yields the exact discontinuity of the tangential magnetic field across S; therefore the high frequency correction expressed by the modal series is continuous in Ω. It is noted that this series converges quite rapidly, its terms going to zero as κ_m^{-4}. Therefore, if we are interested in finding the resonant modes up to a maximum frequency $\omega_{\max}$, we can truncate the modal series, neglecting all the modes having resonant frequencies much larger than $\omega_{\max}$. To guarantee that the truncation error does not affect appreciably the overall accuracy of the algorithm up to the highest frequency of interest, i.e., for $k < k_{\max}$, we shall include in (3) all the modes with $\kappa_m < \alpha k_{\max}$. Their number will be denoted by M. As a matter of fact, a value of α equal to 2 is adequate in most cases, as evidenced by the results shown in Section IV.

We approximate the current density as follows:

$$\vec{J}(\vec{r}\,') = -j\omega\sum_{j=1}^{Q} q_j\vec{v}_j(\vec{r}\,') + \sum_{j=1}^{P} I_j\vec{w}_j(\vec{r}\,') \tag{4}$$

where q_j, I_j are unknown coefficients and $\{\vec{v}_j\}, \{\vec{w}_j\}$ are two sets of linearly independent vector basis-functions defined over S and tangential to it. They satisfy

$$\nabla_s'\cdot\vec{v}_j \neq 0 \;\; ; \;\; \nabla_s'\cdot\vec{w}_j = 0 \tag{5}$$

where $\nabla_s'\cdot$ denotes the surface divergence with respect to the primed coordinates. Since functions $\vec{w}_j$ are solenoidal, the charge density is

$$\sigma(\vec{r}\,') = -\frac{\nabla_s'\cdot\vec{J}(\vec{r}\,')}{j\omega} = \sum_{j=1}^{Q} q_j\nabla_s'\cdot\vec{v}_j(\vec{r}\,'). \tag{6}$$

We assume that also $\{\nabla_s'\cdot\vec{v}_j\}$ constitute a set of linearly independent functions, in order to have $\sigma = 0$ only if all q_j are zero. Due to (4) and (6) coefficients q_j and I_j will be referred to as charges and (solenoidal) currents, respectively. Note that, in the limit $\omega \to 0$, the current density is solenoidal in any case, as it must be.

Furthermore, we introduce the quantities

$$a_m = \frac{jk\sqrt{\epsilon\mu}}{\kappa_m^2(\kappa_m^2-k^2)}\int_S \vec{e}_m\cdot\vec{J}\,dS' \qquad (m = 1,\cdots,M) \tag{7}$$

that are related to the amplitudes of the spherical-cavity modes excited by $\vec{J}$. Coefficients a_m are considered as auxiliary variables, which must be determined together with the charges and the currents. Introducing the charges, the currents and the auxiliary variables into (2), (3), we obtain

$$\vec{E} \approx -\frac{1}{\epsilon}\left[\sum_{j=1}^{Q} q_j\left(\nabla \int_S g\nabla'_s \cdot \vec{v}_j\, dS' + k^2 \int_S \overleftrightarrow{G} \cdot \vec{v}_j\, dS'\right) + jk\sqrt{\epsilon\mu}\sum_{j=1}^{P} I_j \int_S \overleftrightarrow{G} \cdot \vec{w}_j\, dS' + k^2 \sum_{m=1}^{M} a_m \vec{e}_m\right] \quad (8)$$

$$\vec{H} \approx -\frac{j}{\sqrt{\epsilon\mu}}\left[k\sum_{j=1}^{Q} q_j \int_S \nabla\times \overleftrightarrow{G} \cdot \vec{v}_j\, dS' + j\sqrt{\epsilon\mu}\sum_{j=1}^{P} I_j \int_S \nabla\times \overleftrightarrow{G} \cdot \vec{w}_j\, dS' + k\sum_{m=1}^{M} a_m \kappa_m \vec{h}_m\right] \quad (9)$$

where $\vec{h}_m = \nabla \times \vec{e}_m/\kappa_m$ represents the normalized magnetic field vector of the mth mode of the spherical resonator (see [14, p. 308]). The closed-form expression of $\nabla\times \overleftrightarrow{G}$ is given in the Appendix, Section A.

B. The Eigenvalue Problem

Denoting by $\vec{E}_{\tan}$ the component of the electric field tangential to S and using the Galerkin's procedure, the electric wall condition on S results in

$$\int_S \vec{E}_{\tan} \cdot \vec{v}_i\, dS = 0 \qquad (i = 1, \cdots, Q) \quad (10)$$

$$\int_S \vec{E}_{\tan} \cdot \vec{w}_i\, dS = 0 \qquad (i = 1, \cdots, P). \quad (11)$$

These equations, together with the M auxiliary equations (7), can be cast into the matrix form

$$\boldsymbol{K}^4\boldsymbol{a} - k^2\boldsymbol{K}^2\boldsymbol{a} - k^2\boldsymbol{R}'\boldsymbol{q} - jk\sqrt{\epsilon\mu}\ \boldsymbol{R}''\boldsymbol{I} = 0 \quad (12)$$

$$\boldsymbol{S}\boldsymbol{q} - k^2\boldsymbol{R}'^{T}\boldsymbol{a} - k^2\boldsymbol{V}\boldsymbol{q} - jk\sqrt{\epsilon\mu}\ \boldsymbol{Q}\boldsymbol{I} = 0 \quad (13)$$

$$k^2\boldsymbol{R}''^{T}\boldsymbol{a} + k^2\boldsymbol{Q}_T\boldsymbol{q} + jk\sqrt{\epsilon\mu}\ \boldsymbol{W}\boldsymbol{I} = 0 \quad (14)$$

where $_T$ denotes the transpose $\boldsymbol{a} = \{a_1, a_2, \cdots, a_M\}_T, \boldsymbol{q} = \{q_1, q_2, \cdots, q_Q\}_T, \boldsymbol{I} = \{I_1, I_2, \cdots, I_P\}_T, \boldsymbol{K} = \text{diag}\{\kappa_m\}$ and, moreover, the entries of the matrices $\boldsymbol{S}, \boldsymbol{V}, \boldsymbol{W}, \boldsymbol{Q}, \boldsymbol{R}', \boldsymbol{R}''$ are defined as follows:

$$S_{ij} = \int_S\int_S [\nabla_s \cdot \vec{v}_i(\vec{r})]\, g\, [\nabla'_s \cdot \vec{v}_j(\vec{r}\,')]\, dS'\, dS \quad (15)$$

$$V_{ij} = \int_S\int_S \vec{v}_i(\vec{r}) \cdot \overleftrightarrow{G} \cdot \vec{v}_j(\vec{r}\,')\, dS'\, dS \quad (16)$$

$$W_{pq} = \int_S\int_S \vec{w}_p(\vec{r}) \cdot \overleftrightarrow{G} \cdot \vec{w}_q(\vec{r}\,')\, dS'\, dS \quad (17)$$

$$Q_{ip} = \int_S\int_S \vec{v}_i(\vec{r}) \cdot \overleftrightarrow{G} \cdot \vec{w}_p(\vec{r}\,')\, dS'\, dS \quad (18)$$

$$R'_{mi} = \int_S \vec{e}_m(\vec{r}) \cdot \vec{v}_i(\vec{r})\, dS \quad (19)$$

$$R''_{mp} = \int_S \vec{e}_m(\vec{r}) \cdot \vec{w}_p(\vec{r})\, dS \quad (20)$$

where $i, j = 1, \cdots, Q; p, q = 1, \cdots, P$ and $m = 1, \cdots, M$. In the derivation of (15) we used the Gauss' theorem on the closed surface S. All matrices are real and k-independent. The square matrices $\boldsymbol{S}, \boldsymbol{V}$ and $\boldsymbol{W}$ are symmetric, due to the reciprocity of the Green's functions g and $\overleftrightarrow{G}$, and positive definite (see the Appendix, Section C).

System (12)–(14) has nontrivial solutions only for particular values of k, but not all these values are related to resonances in the volume V. First, we note that for $k = 0$ an arbitrary $\boldsymbol{I}$ satisfies system (12)–(14), provided that $\boldsymbol{a} = 0, \boldsymbol{q} = 0$. These solutions correspond to the solenoidal current distributions that, at zero frequency, may exist on the cavity wall. They are not related to resonances and therefore in the following we assume $k > 0$. Next, we observe that the fields associated with any solution of the system (12)–(14) satisfy naturally the electric wall condition on the spherical surface, due to the particular Green's function we used. For this reason, together with the resonant modes of the cavity, we expect to find also the resonances of the complementary region $\Omega - V$, i.e., fields that are zero inside the volume V and that differ from zero in $\Omega - V$. These solution are meaningless and they are easily recognized as discussed in the following.

Since matrix $\boldsymbol{W}$ is nonsingular, it is possible to use (14) to express $\boldsymbol{I}$ as a function of $\boldsymbol{a}$ and $\boldsymbol{q}$

$$-j\sqrt{\epsilon\mu}\boldsymbol{I} = k\boldsymbol{W}^{-1}[\boldsymbol{R}''^{T}\boldsymbol{a} + \boldsymbol{Q}_T\boldsymbol{q}]. \quad (21)$$

Introducing (21) into (12), (13) we obtain a generalized linear eigenvalue problem of the type

$$(\boldsymbol{A} - k^{-2}\boldsymbol{B})\boldsymbol{x} = 0 \quad (22)$$

where

$$\boldsymbol{x} = \begin{bmatrix}\boldsymbol{a}\\ \boldsymbol{q}\end{bmatrix} \quad (23)$$

$$\boldsymbol{A} = \begin{bmatrix}\boldsymbol{K}^2 - \boldsymbol{R}''\boldsymbol{W}^{-1}\boldsymbol{R}''^{T} & \boldsymbol{R}' - \boldsymbol{Q}\boldsymbol{W}^{-1}\boldsymbol{R}''^{T}\\ \boldsymbol{R}'^{T} - \boldsymbol{R}''\boldsymbol{W}^{-1}\boldsymbol{Q}_T & \boldsymbol{V} - \boldsymbol{Q}\boldsymbol{W}^{-1}\boldsymbol{Q}_T\end{bmatrix} \quad (24)$$

$$\boldsymbol{B} = \begin{bmatrix}\boldsymbol{K}^4 & 0\\ 0 & \boldsymbol{S}\end{bmatrix}. \quad (25)$$

Since matrices $\boldsymbol{A}$ and $\boldsymbol{B}$ are real symmetric and definite positive (see the Appendix, Section C), system (22) has positive eigenvalues and real eigenvectors.

Recalling the range of validity of the approximation involved in the truncation of the series in (3), we infer that the only significant eigenvalues of (22) are those larger than $k_{\max}^{-2}$. They correspond to the first resonant frequencies $\omega_r = k_r\sqrt{\epsilon\mu}$ of the cavity and the complementary region $\Omega - V$. Each eigenvector $\boldsymbol{x}_r$ yields directly the mode amplitudes and the charges pertaining to the resonance; the corresponding solenoidal currents are deduced from (21). It is pointed out that no problem arises in finding degenerate modes. Once the mode amplitudes, the charges and the solenoidal currents are known, (8) and (9) yield the resonant fields $\vec{E}_r, \vec{H}_r$ everywhere in Ω. The comparison of the values of the field in a number of points inside and outside V permits one to detect the external resonances and to discard them, since they give rise to a field that theoretically is zero inside V.

C. Orthonormality of the Modal Fields

In the Appendix, Section B, we show that

$$\int_\Omega \vec{H}_r^* \cdot \vec{H}_s \, dV = \frac{1}{\epsilon\mu} \frac{k_r}{k_s} \boldsymbol{x}_{rT} \boldsymbol{B} \boldsymbol{x}_s. \tag{26}$$

When both fields $\vec{H}_r, \vec{H}_s$ pertain to internal resonances, the domain of the integral can be restricted to V, since the fields are virtually zero in the complementary region. On the other hand, standard library routines customarily yield orthonormal eivenvectors satisfying

$$\boldsymbol{x}_{rT} \boldsymbol{B} \boldsymbol{x}_s = \delta_{rs}. \tag{27}$$

Equations (26) and (27) show that the resonant magnetic fields obtained by (9) are orthogonal

$$\int_V \vec{H}_r^* \cdot \vec{H}_s \, dV = \frac{\delta_{rs}}{\epsilon\mu}. \tag{28}$$

Moreover, at resonance the electric and magnetic energy stored in the cavity are equal, at least within the limits of the approximation of the method of moments. Thus (28) permits us to deduce the normalization factors to transform the fields given by (8) and (9) into the normalized vectors $\vec{\mathcal{E}}_r, \vec{\mathcal{H}}_r$ satisfying $\int_V \vec{\mathcal{E}}_r \cdot \vec{\mathcal{E}}_r \, dV = \int_V \vec{\mathcal{H}}_r \cdot \vec{\mathcal{H}}_r \, dV = 1$. We have

$$\vec{\mathcal{E}}_r = \epsilon \vec{E}_r; \quad \vec{\mathcal{H}}_r = -j\sqrt{\epsilon\mu} \vec{H}_r. \tag{29}$$

D. Discretization of the Surface and Choice of the Basis Functions

In our algorithm the surface S is modeled using triangular patches. For simplicity we restrict our analysis to simply connected cavities, bounded by a single conductor and not containing thin conducting sheets. The advantage of using triangular patches for representing complex surfaces is apparent, and it is discussed in detail in a paper by Rao *et al.* [16]. In that paper the authors introduce subdomain basis functions (RWG's b.f.), each one defined over two adjacent triangles [see Fig. 2(a)]. RWG's b.f. have become popular in conjunction with the BIM, since they represent well behaved piecewise-linear current distributions and give rise to zero-mean, piecewise-constant charges. We construct the basis functions $\vec{v}_j$ and $\vec{w}_j$ by a linear combination of the RWG's b.f., in order to retain the same features.

We obtain the generic function $\vec{v}_j$ combining the three RWG's b.f. that share the jth triangle [see Fig. 2(b)]. Thus its support is constituted by the central triangle T_j and the three adjacent triangles $T_{j,h}$. The expression of $\vec{v}_j$ is

$$\vec{v}_j = \begin{cases} \dfrac{1}{2A_j} \vec{\rho}_j & \text{in } T_j \\ -\dfrac{1}{6A_{j,h}} \vec{\rho}_{j,h} & \text{in } T_{j,h} \end{cases} \tag{30}$$

where A_j and $A_{j,h}$ denote the area of the central and the adjacent triangles, respectively, and the other quantities are defined in Fig. 2(b). The function $\vec{v}_j$ represents a current originating at the centroid of the central triangle and flowing towards the external vertices; in the following they will be

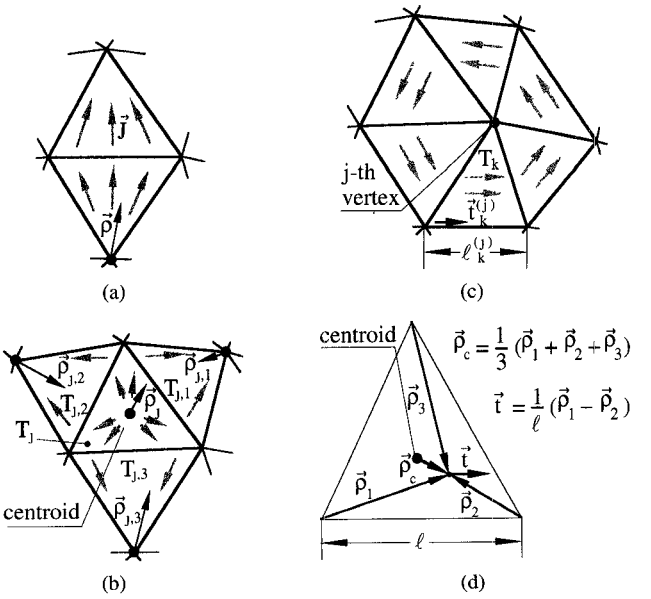

Fig. 2. Vector basis functions suited to represent a current density $\vec{J}$ on triangular patches. (a) a RWG's basis function; (b) a stellate basis function; (c) an annular basis function; (d) geometrical relationships showing that stellate and annular basis functions can be regarded as combinations of RWG's basis functions.

referred to as 'stellate b.f..' The surface divergence of the stellate b.f. is given by

$$\nabla_s' \cdot \vec{v}_j = \begin{cases} \dfrac{1}{A_j} & \text{in } T_j \\ -\dfrac{1}{3A_{j,h}} & \text{in } T_{j,h} \end{cases}. \tag{31}$$

This equation shows that the total charge existing on the central triangle is counterbalanced by three equal charges distributed on the adjacent triangles. It is possible to define as many stellate b.f. as the number N_t of the triangles, but only $N_t - 1$ of them give rise to linearly independent charge distributions. In fact, we can assign independently the charge only on $N_t - 1$ triangles, the last charge being constrained by the total zero-charge condition.

Each function $\vec{w}_j$ is obtained considering the RWG's b.f. relative to all the edges departing from the jth vertex (pivot vertex); its support is constituted by all the triangles T_k sharing the jth vertex [see Fig. 2(c)]. Functions $\vec{w}_j$ are given by

$$\vec{w}_j = \frac{\ell_k^{(j)}}{A_k} \vec{t}_k^{(j)} \quad \text{in } T_k \tag{32}$$

where A_k is the area of T_k, $\ell_k^{(j)}$ is the length of the external edge and $\vec{t}_k^{(j)}$ is the unit vector along that edge [see Fig. 2(c)]. Functions $\vec{w}_j$ represent piecewise-constant currents circulating around their pivot vertices, and hence they will be named 'annular b.f..' It is possible to define as many annular b.f. as the number N_v of the vertices, but only $N_v - 1$ are linearly independent.

Summing up, we define $Q = N_t - 1$ stellate b.f. and $P = N_v - 1$ annular b.f.; the total number of basis functions we consider is $P + Q = N_t + N_v - 2$. On the other hand, the number of the original RWG's b.f. is equal to the number N_e

of the edges that, in turn, is $N_e = N_t + N_v - 2$, according to the Euler's formula valid for any closed polyhedron. The total number of the basis functions we use is therefore equal to that of the RWG's b.f., and the two sets of basis functions are equivalent.

E. Evaluation of the Matrices

The overall accuracy and the numerical efficiency of the algorithm depends largely on the fast and accurate evaluation of the integrals (15)–(18), that requires a double integration over the support of two generic basis functions, and thus involves many pairs of triangles. Actually, taking into account (30)–(32) and the geometric relationships indicated in Fig. 2(d), only two distinct kinds of integrals must be considered, namely

$$I_1 = \int_{T_r} \int_{T_s} g \, dS' \, dS \tag{33}$$

$$I_2 = \int_{T_r} \int_{T_s} \vec{\rho}_r(\vec{r}) \cdot \overrightarrow{G} \cdot \vec{\rho}_s(\vec{r}\,') \, dS' \, dS. \tag{34}$$

In these equations T_r, T_s are a generic pair of triangles and $\vec{\rho}_r, \vec{\rho}_s$ are the position vectors of the field and source points, relative to a generic vertex of T_r and T_s, respectively. Integrals in the form I_1 result after substituting (31) into (15), whereas integrals in the form I_2 are encountered in the evaluation of coefficients (16)–(18). It is worth noting that, since many pairs of basis functions share the same pair of triangles, each one of the integrals I_1 and I_2 is needed in the evaluation of many matrix elements. Therefore, as pointed out in [16], it is by far more efficient to carry out the evaluation of the matrix elements using a scheme based on triangle-pair combinations, rather than computing them naively. In a forthcoming paper [17] we address the issue of achieving a good trade-off between accuracy and computing time in the evaluation of I_1 and I_2. In that paper we discuss the Gaussian integration scheme best suited for the numerical integration and we report, for coincident T_r and T_s, the analytical expressions of the parts of integrals I_1 and I_2 which derive from the singular terms of g and $\overleftrightarrow{G}$ (see A-1, A-3).

The evaluation of the integrals (19) and (20) is less critical, since the integrand functions are always bound and a single surface integration is needed. Thus Gaussian quadrature formulas are adequate.

III. The Computer Code

The algorithm has been implemented in a computer code named MORESCA (MOdes of RESonant CAvities). The input consists of a formatted file containing the coordinates of the vertices of the triangular patches and the topological information about the mesh, together with the permittivities of the medium and the frequency $\omega_{\max}$. The definition of the geometry and the generation of the surface mesh may be performed with the help of a commercial mechanical CAD code (PATRAN), to which an interface is available. The first step is the evaluation of the matrix coefficients: integrals (33), (34) are evaluated for each pair of triangles and then they are accumulated in the appropriate elements of the matrices $\boldsymbol{S}, \boldsymbol{V}, \boldsymbol{W}, \boldsymbol{Q}$. A point that deserves some attention is the calculation of the coefficients depending on the dyadic $\overrightarrow{G}$, whose expression is rather complicated, as evidenced by (A-3)–(A-8). We found that the evaluation of the functions f_1, f_2, f_3, f_4, defined by (A-9)–(A-12), is quite long. On the other hand, these functions are fairly smooth and depend only on the two quantities h and u defined in the Appendix, Section A; thus it is convenient the use of look-up tables to calculate them. We found that only 200 entries per table are sufficient, and that the use of the tables reduces the computation time of the matrices $\boldsymbol{V}, \boldsymbol{W}$ and $\boldsymbol{Q}$ by a factor of four.

The number M of the resonant modes of the spherical region to be taken into account in the calculation of the matrices $\boldsymbol{R}'$ and $\boldsymbol{R}''$ is determined automatically, considering all resonances up to $\alpha\omega_{\max}$. The value of the parameter α is chosen by making a trade-off between accuracy and speed: it is customarily set to 2, and it can be increased if a better accuracy is needed (see next section).

The eigenvalue problem (22) is solved using the LAPACK routines [18].

The selection of the resonances of the internal region V is performed automatically. For each eigensolution of (22) the code compares the magnitudes of the magnetic field calculated at the centroid of a number of triangles, immediately inside and outside the surface S. If the mean value of the external field is much larger than that of the internal one, the solution is discarded. The eigenvalues and the corresponding eigenvectors are stored in a file to be used by post-processing programs for calculating normalized fields, Q-factors, shunt impedances and so on.

In the frequent cases where the cavity has one or more reflection symmetries, it is possible to reduce the dimension of the problem and the CPU time by considering a current sheet defined only over the significant part of the cavity wall. In these cases the modes belonging to different symmetry classes are obtained solving different problems, one for each class. Minor changes on the definitions of the basis functions are needed, to impose the required symmetry to the current. When calculating matrices $\boldsymbol{S}, \boldsymbol{V}, \boldsymbol{W}$ and $\boldsymbol{Q}$, many intermediate results, not depending on the particular class of symmetry, can be stored and reused, with a substantial saving of CPU time.

IV. Numerical Results

The accuracy of the results is affected by the truncation of the series in (3) and by the approximations done in representing $\vec{J}$ and in discretizing S. Obviously, the finer is the mesh, the better are these last approximations; furthermore, the larger is the parameter α, the smaller is the truncation error. To reduce the CPU time, however, the number of triangles in the mesh and the value of α must be set to the minimum compatible with the desired accuracy. To get a quantitative insight on this topic, we performed many test calculations on rectangular, spherical and cylindrical cavities to compare the theoretical values of the resonant frequencies of a large number of modes with those calculated with different meshes and different α. We limit ourselves to report the results for a rectangular cavity, since in this case the mesh size affects the representation of $\vec{J}$ only, and not that of the surface.

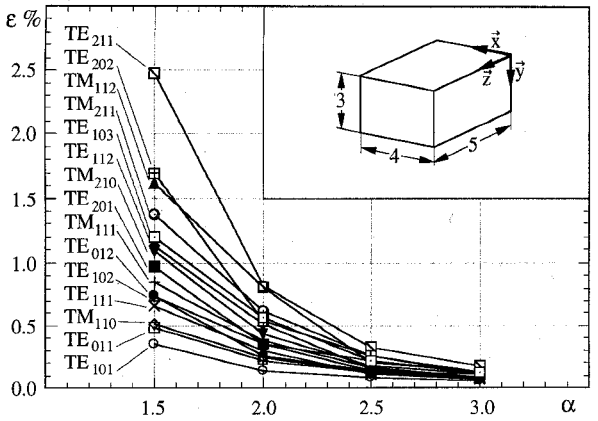

Fig. 3. Magnitude of the relative error ϵ in the calculation of the first 15 resonant frequencies of a rectangular cavity for different values of the parameter α. The dimensions shown are in cm.

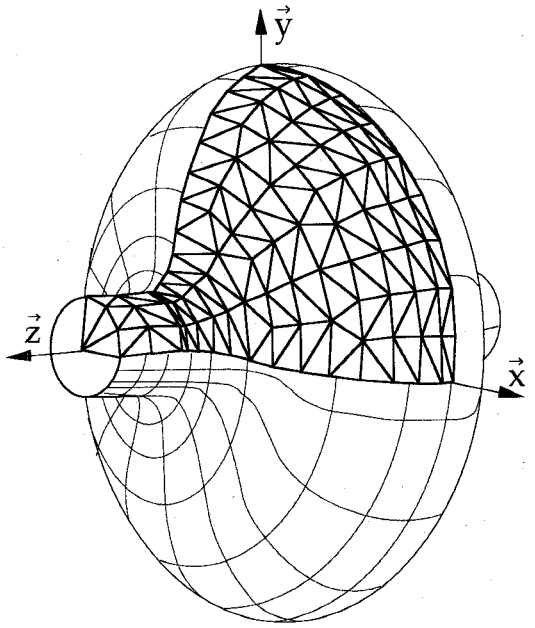

Fig. 4. The ELETTRA accelerating cavity. The mesh shown is that used to obtain the results of Table I.

TABLE I
RESONANT FREQUENCIES OF THE FIRST 12 MODES OF THE ELETTRA CAVITY. SYMMETRIES: e = EVEN; o = ODD

Symmetry x y z	Resonant Frequencies [MHz] Calculated	Measured	% errors
e e o	501.73	500.11	0.32
o e e ; e o e	747.61	753.44	-0.77
e o o ; o e o	749.45	748.28	0.16
e e e ; o o e	936.43	942.32	-0.63
e e e	948.62	956.55	-0.83
e e o ; o o o	994.90	991.03	0.39
o o e	1005.0	1009.4	-0.44
e e o	1064.0	1062.8	0.11

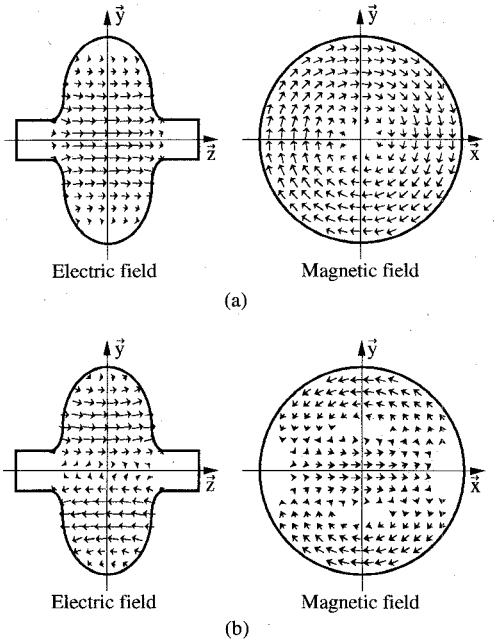

Fig. 5. Arrow plots representing two resonant fields of the ELETTRA cavity. (a) Fundamental mode; (b) first deflecting mode.

The influence of α is shown in Fig. 3, which reports the magnitude of the relative error in the determination of the resonant frequencies of the cavity shown in the same figure. The cavity was analyzed up to 10 GHz, and in this band a total of 15 resonances are found, from the TE_{101} mode (resonating at 4.799 GHz) to the TE_{103} mode (9.744 GHz). A rather fine mesh, consisting of 94 triangles, was used to model one eighth of the cavity wall (the symmetries were taken into account). The values of α equal to 1.5, 2, 2.5, and 3 were considered, that caused the number M for each symmetry class to be about 25, 65, 125, and 210, respectively. As expected, the overall accuracy increased with increasing α. Computing time increased too; it took about 5.5, 8, 12, and 20 minutes on a DIGITAL VAXstation 4000/60 to perform, for each values of α, the calculations relative to all the symmetry classes. It is apparent that $\alpha = 2$, which yields an accuracy better than 1% for all the resonant frequencies, can be considered a good compromise. The tests performed to check the influence of the mesh size, not reported for brevity, showed that an accuracy better than 0.3% is obtained if the dimensions of the edges do not exceed one quarter of the wavelength at $\omega_{\max}$.

We finally report the results of a test calculation, that refers to the 500 MHz accelerating cavity shown in Fig. 4, and used in the Trieste Synchrotron Light Source ELETTRA. The symmetry permitted us to model only one eighth of the surface, using a mesh consisting of 165 triangles (see Fig. 4). The wide-band analysis of this cavity evidenced the efficiency of the code: in fact, only 30 minutes of CPU time were needed to calculate the 90 modes up to 2 GHz, i.e., up to four times the frequency of the fundamental mode ($\alpha = 2$ was used). In Table I the calculated resonant frequencies of the first few modes, for which experimental data are available, are compared with the measured values. The modes are classified according to their even or odd symmetry with respect to the coordinate planes, and rotationally degenerate modes are considered together. A good agreement between calculated and experimental values is obtained. The arrow plots of Fig. 5 represent the field patterns of the dominant (accelerating) mode and of the first deflecting mode. For the accelerating mode we calculated a Q-factor equal to 44 300 (assuming copper wall) and a value of R_s/Q

(the ratio of the shunt impedance to the Q-factor) equal to 175.6 Ω. Also these values compare well with the measured ones, which are $Q_{\text{meas}} = 42000$ and $(R_s/Q)_{\text{meas}} = 174.5\,\Omega$.

V. Conclusion

We presented an efficient algorithm, based on the boundary integral method, for the mode analysis of arbitrarily shaped resonators. Its peculiarity lies in the fact that all the resonances of interest are obtained solving a matrix linear eigenvalue problem. Computing time is moderate, even when many resonances must be found; no *a priori* guess of the resonant frequencies is required and no problem arises in the case of degenerate modes. Finally, the normalized fields are obtained with no additional computational effort: thus the algorithm is particularly attractive when the fields must be post-processed to evaluate some global parameters used in the characterization of accelerator cavities (e.g., Q-factors, beam coupling impedances, etc.) or, in general, when the resonant fields are used in modal expansions.

Appendix

A. Expressions for Functions g and $\overleftrightarrow{G}$

The expressions for g and $\overleftrightarrow{G}$ can be written in a compact form referring them to the coordinate system reported in [10], i.e.\ considering the unit vectors $\vec{r}_0 = \vec{r}/|\vec{r}|, \vec{r}\,'_0 = \vec{r}\,'/|\vec{r}\,'|, \vec{t}_0 = \vec{r}\,'_0 \times \vec{r}_0/|\vec{r}\,'_0 \times \vec{r}_0|, \vec{s}_0 = \vec{t}_0 \times \vec{r}_0$ and $\vec{s}\,'_0 = \vec{t}_0 \times \vec{r}\,'_0$. Denoting by a the radius of the sphere and by ψ the angle between $\vec{r}$ and $\vec{r}\,'$, we define: $\vec{R} = \vec{r} - \vec{r}\,', r = |\vec{r}|, r' = |\vec{r}\,'|, R = |\vec{R}|, h = rr'/a^2, \xi = 1 - r^2/a^2, \xi' = 1 - r'^2/a^2, u = \cos\psi$ and $v = \sqrt{1-u^2}$.

The function g is

$$g = \frac{1}{4\pi R} - \frac{1}{4\pi a} f_0 \tag{A-1}$$

where $f_0 = 1/\sqrt{1-2hu+h^2}$.

The dyadic $\overleftrightarrow{G}$ has the following eigenfunction expansion:

$$\overleftrightarrow{G} = \sum_{i=1}^{\infty} \frac{\vec{e}_i(\vec{r})\vec{e}_i(\vec{r}\,')}{\kappa_i^2}. \tag{A-2}$$

The closed form of $\overleftrightarrow{G}$ can be found in [10], and it is reported here in a form that is more convenient for numerical evaluation. We have

$$\overleftrightarrow{G} = \frac{1}{8\pi R}\left(\vec{I} + \frac{\vec{R}\vec{R}}{R^2}\right) + \overleftrightarrow{G}^0 \tag{A-3}$$

where $\overleftrightarrow{G}^0$ is a regular dyadic that, thanks to the choice of the reference system, has only five nonzero components

$$\begin{aligned}\overleftrightarrow{G}^0 = {} & \vec{r}_0\vec{r}\,'_0 G^0_{rr'} + \vec{r}_0\vec{s}\,'_0 G^0_{rs'} + \vec{s}_0\vec{r}\,'_0 G^0_{sr'} \\ & + \vec{s}_0\vec{s}\,'_0 G^0_{ss'} + \vec{t}_0\vec{t}_0 G^0_{tt}.\end{aligned}$$

They have the following expressions

$$\begin{aligned} G^0_{rr'} = {} & f_0/(4\pi a)[(15 + h^2 - 3\xi - 3\xi')f_1 + f_2 \\ & + (h - 3u)/4 - f_0^2(\xi + \xi')(h - u)/4] \end{aligned} \tag{A-4}$$

$$\begin{aligned} G^0_{rs'} = {} & -v\xi' f_0^2/(4\pi a)[(2 - \xi/2)f_3 + f_4] \\ & - vf_0/(16\pi a)[3 - (\xi + \xi')f_0^2] \end{aligned} \tag{A-5}$$

$$\begin{aligned} G^0_{ss'} = {} & \xi\xi' f_0^2/(4\pi a)[3f_1/f_0 - u(f_3 + f_4) \\ & - f_0(h - u)/4] - f_0/(8\pi a)[u + hv^2 f_0^2] \end{aligned} \tag{A-6}$$

$$G^0_{tt} = f_0/(4\pi a)[\xi\xi' f_0(f_3 + f_4) - 1/2] \tag{A-7}$$

$$G^0_{sr'}(r, r') = -G^0_{rs'}(r', r) \tag{A-8}$$

where

$$f_1 = \frac{1}{8hf_0}\left[f_0 - \frac{3}{h(1+h)}\left(\frac{F - 2E}{\sin\beta} + \frac{1}{f_0}\right)\right] \tag{A-9}$$

$$f_2 = 1/(h^2 f_0)[\ln(1/f_0 + h - u) - \ln(1 - u) - hf_0] \tag{A-10}$$

$$\begin{aligned} f_3 = {} & 1/[4v^2h^2(1+h)f_0^2]\{(1+u)(1+h-2hu)f_0 \\ & - [(1-u)F + 2uE]/\sin\beta\} \end{aligned} \tag{A-11}$$

$$f_4 = 1/(v^2h^2f_0^2)[1 + (hu - 1)f_0] \tag{A-12}$$

and $F = F(\beta, K), E = E(\beta, K)$ denote the incomplete elliptic integrals of the first and of the second kind, respectively, having argument $\beta = \arcsin 2\sqrt{h}/(1+h)$ and modulus $K = \sqrt{(1+u)/2}$.

The eigenfunction expansion of $\nabla\times\overleftrightarrow{G}$ is

$$\nabla\times\overleftrightarrow{G} = \sum_{i=1}^{\infty} \frac{\vec{h}_i(\vec{r})\vec{e}_i(\vec{r}\,')}{\kappa_i} \tag{A-13}$$

and its closed-form expression, deduced from (A-3), is

$$\nabla\times\overleftrightarrow{G} = -\frac{1}{4\pi R^3}\vec{R}\times\vec{I} + \nabla\times\overleftrightarrow{G}^0 \tag{A-14}$$

where

$$\begin{aligned} \nabla\times\overleftrightarrow{G}^0 = {} & f_0^2/(4\pi ar')\{v(1-\xi')f_0\vec{r}_0\vec{t}_0 \\ & + hv(f_0 - f_4)\vec{t}_0\vec{r}\,'_0 \\ & + [\xi' hf_4 - (1-\xi')(h-u)f_0]\vec{s}_0\vec{t}_0 \\ & + [\xi'(1/f_0 + huf_4) + (hu-1)f_0]\vec{t}_0\vec{s}\,'_0\}. \end{aligned} \tag{A-15}$$

B. Derivation of (26)

Let us consider two magnetic fields $\vec{H}_\alpha$ and $\vec{H}_\beta$ in Ω, produced by the current densities $\vec{J}_\alpha$ and $\vec{J}_\beta$ distributed on S (in the following the subscripts α and β will refer to quantities related to $\vec{J}_\alpha$ and $\vec{J}_\beta$, respectively). Taking into account (1)–(3) and (7) we have

$$\mathcal{I} = \int_\Omega \vec{H}^*_\alpha \cdot \vec{H}_\beta\, dV = \mathcal{I}_1 + \mathcal{I}_2 + \mathcal{I}_3 + \mathcal{I}_4 \tag{A-16}$$

where

$$\mathcal{I}_1 = \int_\Omega \left(\int_S \nabla \times \overleftrightarrow{G} \cdot \vec{J}_\alpha^* \, dS' \right) \cdot \left(\int_S \nabla \times \overleftrightarrow{G} \cdot \vec{J}_\beta \, dS' \right) dV$$

$$\mathcal{I}_2 = j\omega_\beta \int_\Omega \left(\int_S \nabla \times \overleftrightarrow{G} \cdot \vec{J}_\alpha^* \, dS' \right) \cdot \sum_{m=1}^{M} a_{\beta m} \kappa_m \vec{h}_m \, dV$$

$$\mathcal{I}_4 = \omega_\alpha \omega_\beta \int_\Omega \sum_{m=1}^{M} a_{\alpha m}^* \kappa_m \vec{h}_m \cdot \sum_{n=1}^{M} a_{\beta n} \kappa_n \vec{h}_n \, dV$$

and $\mathcal{I}_3$ is the conjugate of $\mathcal{I}_2$ with α and β interchanged. From the eigenfunction expansion of $\nabla \times \overleftrightarrow{G}$ (A-13) we have

$$\int_S \nabla \times \overleftrightarrow{G} \cdot \vec{J} \, dS' = \sum_{i=1}^{\infty} \frac{\vec{h}_i}{\kappa_i} \int_S \vec{e}_i \cdot \vec{J} \, dS'.$$

Thus, taking into account the orthonormality of vectors $\vec{h}_i$, using (A-2) and substituting (4) and (16)–(18), we have

$$\mathcal{I}_1 = \boldsymbol{I}_{\alpha T}^* \boldsymbol{W} \boldsymbol{I}_\beta - j\omega_\alpha \boldsymbol{q}_{\alpha T}^* \boldsymbol{Q} \boldsymbol{I}_\beta + j\omega_\beta \boldsymbol{I}_{\alpha T}^* \boldsymbol{Q}_T \boldsymbol{q}_\beta + \omega_\alpha \omega_\beta \boldsymbol{q}_{\alpha T}^* \boldsymbol{V} \boldsymbol{q}_\beta \quad \text{(A-17)}$$

$$\mathcal{I}_2 = \omega_\alpha \omega_\beta \boldsymbol{a}_{\beta T} \boldsymbol{R}' \boldsymbol{q}_\alpha^* + j\omega_\beta \boldsymbol{a}_{\beta T} \boldsymbol{R}'' \boldsymbol{I}_\alpha^* \quad \text{(A-18)}$$

$$\mathcal{I}_4 = \omega_\alpha \omega_\beta \boldsymbol{a}_{\alpha T}^* \boldsymbol{K}^2 \boldsymbol{a}_\beta. \quad \text{(A-19)}$$

Introducing (21) into the above expressions, (A-16) becomes

$$\begin{aligned} \mathcal{I} = \omega_\alpha \omega_\beta [& \boldsymbol{a}_{\alpha T}^* (\boldsymbol{K}^2 - \boldsymbol{R}'' \boldsymbol{W}^{-1} \boldsymbol{R}_T'') \boldsymbol{a}_\beta \\ & + \boldsymbol{a}_{\alpha T}^* (\boldsymbol{R}' - \boldsymbol{R}'' \boldsymbol{W}^{-1} \boldsymbol{Q}_T) \boldsymbol{q}_\beta \\ & + \boldsymbol{q}_{\alpha T}^* (\boldsymbol{R}_T' - \boldsymbol{Q} \boldsymbol{W}^{-1} \boldsymbol{R}_T'') \boldsymbol{a}_\beta \\ & + \boldsymbol{q}_{\alpha T}^* (\boldsymbol{V} - \boldsymbol{Q} \boldsymbol{W}^{-1} \boldsymbol{Q}_T) \boldsymbol{q}_\beta] \end{aligned}$$

or, taking into account (23), (24)

$$\int_\Omega \vec{H}_\alpha^* \cdot \vec{H}_\beta \, dV = \frac{k_\alpha k_\beta}{\epsilon \mu} \boldsymbol{x}_{\alpha T}^* \boldsymbol{A} \boldsymbol{x}_\beta. \quad \text{(A-20)}$$

When $\boldsymbol{x}_\alpha, k_\alpha$ and $\boldsymbol{x}_\beta, k_\beta$ are eigensolutions of system (22), the right-hand side of (A-20) can be transformed using (22), and (26) is obtained.

C. Positive Definiteness of Matrices $\boldsymbol{S}, \boldsymbol{A}, \boldsymbol{V}, \boldsymbol{W}$

The electrostatic energy pertaining to a surface charge density σ distributed on S is given by $U_E = 1/2 \int_S \sigma \Phi \, dS$. Taking into account (2), (6), and (15), we have $U_E = (1/2\epsilon) \boldsymbol{q}_T \boldsymbol{S} \boldsymbol{q}$. Therefore the matrix S is positive definite, since U_E is always positive.

If we put $\vec{H}_\alpha = \vec{H}_\beta = \vec{H}$ in (A-16), $\mathcal{I}$ and $\mathcal{I}_1$ become positive quantities, and (A-20), (A-17) represent the quadratic form associated to the matrices $\boldsymbol{A}$ and $[\{\boldsymbol{W}, \boldsymbol{Q}\}, \{\boldsymbol{Q}_T, \boldsymbol{V}\}]$, respectively. Therefore matrix $\boldsymbol{A}$ is positive definite, together with matrices $\boldsymbol{V}$ and $\boldsymbol{W}$, that are principal minors of a positive definite matrix.

ACKNOWLEDGMENT

The authors wish to thank Prof. G. Conciauro for fruitful discussions.

REFERENCES

[1] P. Arcioni, M. Bressan, and G. Conciauro, "Wideband analysis of planar waveguide circuits," *Alta Frequenza*, special issue "Focus on computer oriented design techniques for microwave circuits," vol. LVII, no. 5, pp. 217–226, June 1988.

[2] ——, "A new algorithm for the wideband analysis of arbitrarily shaped planar circuits," *IEEE Trans. Microwave Theory Tech.*, vol. 36, no. 10, pp. 1426–1437, Oct. 1988.

[3] P. Arcioni and G. Conciauro, "Feasibility of HOM-free accelerating resonators: basic ideas and impedance calculations," *Particle Accelerators*, vol. 36, pp. 177–203, 1991.

[4] J.-S. Wang and N. Ida, "Eigenvalue analysis in electromagnetic cavities using divergence free finite elements," *IEEE Trans. Magn.*, vol. 27, no. 5, pp. 3978–3981, 1991.

[5] I. Bardi, O. Biro, and K. Preis, "Finite element scheme for 3-D cavities without spurious modes," *IEEE Trans. Magn.*, vol. 27, no. 5, pp. 4036–4039, 1991.

[6] K. Sakiyama, H. Kotera, and A. Ahagon, "3-D electromagnetic field mode analysis using finite element method by edge element," *IEEE Trans. Magn.*, vol. 26, no. 5, pp. 1759–1761, 1990.

[7] M. Dehler *et al.*, "Status and future of the 3D MAFIA group of codes," *IEEE Trans. Magn.*, vol. 26, no. 2, pp. 751–754, 1990.

[8] M. de Jong and F. Adams, "Cavity RF mode analysis using a boundary-integral method," in *Proc. Particle Accelerator Conf. (PAC93)*, Washington, DC, May 17–20, 1993, pp. 935–937.

[9] J. B. Davies, "The finite element method," in *Numerical Techniques For Microwave and Millimeter Wave Passive Structures*, T. Itoh, Ed. New York: Wiley, 1989, ch. 2., section 7.3-4.

[10] M. Bressan and G. Conciauro, "Singularity extraction from the electric Green's function for a spherical resonator," *IEEE Trans. Microwave Theory Tech.*, vol. MTT-33, no. 5, pp. 407–414, May 1985.

[11] M. Bressan, G. Conciauro, and C. Zuffada, "Waveguide modes via an integral equation leading to a linear matrix eigenvalue problem," *IEEE Trans. Microwave Theory Tech.*, vol. MTT-32, no. 11, pp. 1495–1504, Nov. 1984.

[12] P. Arcioni, M. Bressan, and L. Perregrini, "A new 3-D electromagnetic solver for the design of arbitrarily shaped accelerating cavities," in *Proc. Particle Accelerator Conf. (PAC93)*, Washington, DC, May 17–20, 1993, pp. 772–774.

[13] ——, "A new algorithm for the modal analysis of 3-D arbitrarily shaped resonant cavities," in *Proc. 23rd European Microwave Conf.*, Madrid, Sept. 6–9, 1993, pp. 330–333.

[14] J. Van Bladel, *Electromagnetic Fields*. Washington, DC: Hemisphere, 1985.

[15] ——, *Singular Electromagnetic Fields and Sources*. Oxford: Clarendon Press, 1991.

[16] S. M. Rao, D. R. Wilton, and A.W. Glisson, "Electromagnetic scattering by surfaces of arbitrary shape," *IEEE Trans. Antennas Propagat.*, vol. AP-30, no. 3, pp. 409–418, May 1982.

[17] P. Arcioni, M. Bressan, and L. Perregrini, "On the evaluation of the double surface integrals arising in the application of the Boundary Integral Method to 3-D problems," *IEEE Trans. Microwave Theory Tech.*, submitted.

[18] E. Anderson, *et al.*, *LAPACK, User's Guide*. Philadelphia: SIAM, 1992.

Paolo Arcioni (M'95) was born in Busto Arsizio, Italy, in 1949. He received the degree in electronic engineering from the University of Pavia, Italy, in 1973.

He joined the Department of Electronics of the University of Pavia as a Researcher in electromagnetics, and he has taught a course in microwave theory as an Associate Professor there since 1976. His current research interests concern the development of numerical methods for the electromagnetic CAD of passive microwave circuits. In 1990 he spent a period as Visiting Scientist at the Stanford Linear Accelerator Center, CA, where he was involved with the RF group in the design of optimized cavities for the PEP II project. At present he works with the National Laboratories of Frascati, Italy, in the design of the accelerating cavities for the DAΦNE storage ring.

Mr. Arcioni is a member of the AEI.

Marco Bressan (M'93) was born in Venice, Italy, in 1949. He received the degree in electronic engineering from the University of Pavia in 1972.

Since 1973 has been with the Department of Electronics of the University of Pavia, as a Researcher in the field of electromagnetics. In 1987 he joined the Faculty of Engineering of the University of Pavia, where he teaches on antennas and propagation as an Associate Professor. His current research interests are in antenna theory and in analytical and numerical techniques for electromagnetics. At present he is responsible for the formulation of numerical general algorithms for the wide band analysis of 3-D passive microwave circuits including homogeneous or stratified media.

Luca Perregrini was born in Sondrio, Italy, in 1964. He received the degree in electronic engineering and the Ph.D. degree from the University of Pavia in 1989 and 1993, respectively. His Ph.D. thesis dealt with the development of a new algorithm for the analysis of arbitrarily shaped cavity resonators.

In 1992 he joined the Department of Electronics of the University of Pavia as a Researcher in electromagnetics. His current research interests are devoted to the development of numerical methods for the analysis of waveguide circuits.